frontiers | Frontiers in Materials

TYPE Original Research
PUBLISHED 06 July 2023
DOI 10.3389/fmats.2023.1219688

OPEN ACCESS

EDITED BY
Nicola Maria Pugno,
University of Trento, Italy

REVIEWED BY
Wang Xiaoqiang,
Shenyang Aerospace University, China
Andreas Schiffer,
Khalifa University, United Arab Emirates

*CORRESPONDENCE
Seunghwa Ryu,
ryush@kaist.ac.kr

RECEIVED 09 May 2023
ACCEPTED 21 June 2023
PUBLISHED 06 July 2023

CITATION
Yeo J, Jung J and Ryu S (2023), Coarse-grained modeling for predicting the piezoresistive response of CNT-elastomer nanocomposite. *Front. Mater.* 10:1219688. doi: 10.3389/fmats.2023.1219688

Coarse-grained modeling for predicting the piezoresistive response of CNT-elastomer nanocomposite

Jinwook Yeo[1], Jiyoung Jung[1,2] and Seunghwa Ryu[1]*

[1]Department of Mechanical Engineering, Korea Advanced Institute of Science and Technology (KAIST), Daejeon, Republic of Korea, [2]Department of Mechanical Engineering, University of California, Berkeley, Berkeley, CA, United States

Significant attention has been paid to developing highly flexible and highly stretchable strain sensors due to the increasing demand for wearable devices such as motion-capturing devices and health-monitoring devices. Especially, carbon nanotube (CNT) network-based elastomeric sensors have been studied extensively for their unique strong piezoresistive response under large deformation. Despite its importance for the facile design of sensors, the effect of length and volume fraction of CNT on the piezoresistivity over a large strain range has not been fully uncovered. In this study, by combining coarse-grained molecular statics (CGMS) simulations and efficient percolation network analysis, we investigate the piezoresistive response of the CNT network for a wide range of the length and volume fraction and visualized the CNT network topology to understand the mechanism behind the piezoresistivity response. Based on the set of calculations, we obtain the design map of stretchability and sensitivity for the CNT-elastomer nanocomposite sensors over a wide range of design parameters of CNT, which can be used to fabricate the strain sensor with a desired performance.

KEYWORDS

piezoresistive effect, percolation network, coarse-grained molecular statics, CNT-elastomer nanocomposite, numerical simulation

1 Introduction

The demands for flexible and wearable strain sensors are increasing for versatile applications such as motion-capturing devices, human health monitoring devices, and structural monitoring systems (Lorussi et al., 2005; Yamada et al., 2011; Amjadi et al., 2014; Farooq and Sazonov, 2015; Kwon et al., 2016; Huo et al., 2019; Lu et al., 2019). Therefore, significant efforts have been made to develop strain sensors to meet the requirements of various engineering applications concerning the sensitivity, stretchability, or combination of both (Liu and Choi, 2009; Helmer et al., 2011; Xiao et al., 2011; Zhang et al., 2011; Lu et al., 2012; Wang et al., 2015). One of the promising candidate materials for stretchable strain sensors is the carbon nanotube (CNT) reinforced elastomer nanocomposite which exploits the superior mechanical and electrical properties of CNT. In the nanocomposite, the CNTs form percolation networks that endow electrical conductivity (Kang et al., 2006; Obitayo and Liu, 2012; Sun et al., 2020), and the topology change of the percolation network under mechanical loading leads to the piezoresistive response. Because of the persistent percolation

network made of CNTs, the nanocomposites can sustain conductivity under large stretches, which makes them a promising candidate for highly flexible and highly stretchable strain sensors.

It is reported that, in general, the stretchability and sensitivity of sensors are in a trade-off relationship (Song et al., 2018), and the same is true for nanocomposite sensors. If we can properly tune the two characteristics in a trade-off relationship, appropriate CNT-elastomer nanocomposite sensors can be designed for the desired purpose. For this purpose, many studies have been conducted to investigate the piezoresistive effect of the nanocomposite (Hu et al., 2008; Seidel and Lagoudas, 2009; Haghgoo et al., 2020). Theoretical and computational modeling have been conducted extensively to deepen the microscopic origin behind the piezoelectric response (Jung et al., 2019; Mora et al., 2020).

In computational simulations, the topological change of CNT networks under stretch is predicted, and then the resulting resistance change is computed based on percolation analyses (Grujicic et al., 2004; Li and Kim, 2007). The mechanical behavior of CNTs is affected by embedding medium significantly. When CNT networks are embedded in the elastomer as shown in Figure 1A, the response of CNT is rather constrained due to the polymer matrix. By considering the high ratio between Young's moduli of CNTs and the elastomeric matrix, one can describe the CNT network change based on the affine transformation that preserves a ratio of the distance between any pairs of points (Taya et al., 1998; Hu et al., 2012). This is capable of fast calculation for various cases, which allows the investigation of a wide range of alignment, the volume fraction of CNT, strain range, and so on (Hu et al., 2011; Njuguna et al., 2012; De Vivo et al., 2014). On the other hand, when the CNT network is formed on the polymer substrate as shown in Figure 1B, CNT-to-CNT interaction based on van der Waals forces becomes dominant and CNTs could move much more freely, which can not be modeled by affine transformation unlike in the former case. Lihuan Jin et al. (Jin et al., 2018) introduced coarse-grained molecular statics (CGMS) simulations to exploit the CNT network change considering the interaction between CNTs and determined the resistance change of nanocomposite over deformation. Although their study revealed the key factor determining the piezoresistivity of CNT networks, a wider range of volume fraction of CNT, length of CNT, and strain must be explored to design highly stretchable sensors with desired properties.

In this research, we develop an efficient analysis method for analyzing CNT percolation network in the nanocomposites. And, we applied the method for obtaining the piezoresistive sensor performance in a wide range of volume fractions and lengths of CNT under large stretches. We construct the CNT network on a polymer substrate as shown in Figure 2A and employ molecular statics simulation with a coarse-grained force field for intra-CNT and inter-CNT interactions, which makes us to invest more real-like CNT behavior (Levitt, 1976; Gorban and Karlin, 2002; Chen et al., 2011). By adopting a sparse matrix and depth-first search (DFS) algorithm, we significantly reduced the computational time for obtaining percolation analysis compared to existing methods (Lee et al., 2015; Jung et al., 2020), which permits us to consider a large strain range at a low computational cost. The proposed model is utilized to reveal the piezoresistive response of CNT-elastomer nanocomposites over a wide range of length and volume fraction of CNT, and the microscopic origin of the piezoresistive response was analyzed by visualizing the CNT network topology. Last, we provide a design map that can be used as a reference to fabricate CNT-elastomer nanocomposite sensors.

2 Methods

We perform two numerical analyses in series to predict the piezoresistive response of a CNT-elastomer nanocomposite. First, a CGMS simulation modeling is performed to obtain the CNT network topology on an elastomeric substrate over the stretch. Second, the percolation network analysis is performed to analyze the connectivity between CNTs, find the percolating networks, and calculate the effective conductivity of the CNT network.

2.1 Preparation of initial distribution of CNTs

The initial distribution of CNTs is randomly assigned, whereas straight CNTs were considered for convenience. When the geometric properties such as length, volume fraction of CNT, and elastomeric substrate size are given, initial positions and orientations of CNTs, who is as, are randomly chosen as depicted in Figure 2B. To reduce statistical errors originating from the randomly assigned initial CNT networks, for each design parameter set, i.e., length and volume fraction of CNT, 10 different samples are generated and analyzed, and the averaged conductance values at each strain are obtained as shown in Figure 2E.

2.2 CGMS simulation model for CNT network topology

To analyze the distribution and behavior of CNT according to external deformation, Large-scale Atomic/Molecular Massively Parallel Simulator (LAMMPS) is utilized for atomistic simulation, in which the stable configuration of CNTs is obtained through the energy minimization (Plimpton, 1995). Due to the high computational cost of full atomistic simulations, CGMS simulation was introduced for modeling CNT network. In the CGMS simulation model, several atoms or molecules are lumped into a bead as shown in Figure 1C, so that the system's degree of freedom can be greatly reduced (Fish et al., 2021). For the newly defined beads, the interaction between beads must be defined. In this research, axial direction interaction between two beads in the same CNT, bending interaction between three beads in the same CNT, and interaction between two beads in different CNTs are considered. The interactions are implemented in the model through interatomic potential functions, and the model parameters are determined through a comparison between CGMS and full atomistic simulation (Buehler, 2006), as shown in Table 1 which is calculated under the assumption that the two beads' equilibrium distance is 10 Å. Besides, the conjugate gradient method is adopted as a minimization method, and the convergence criterion is defined as follows,

$$\left|\frac{E_i - E_{i+1}}{E_i}\right| < 10^{-8} \tag{1}$$

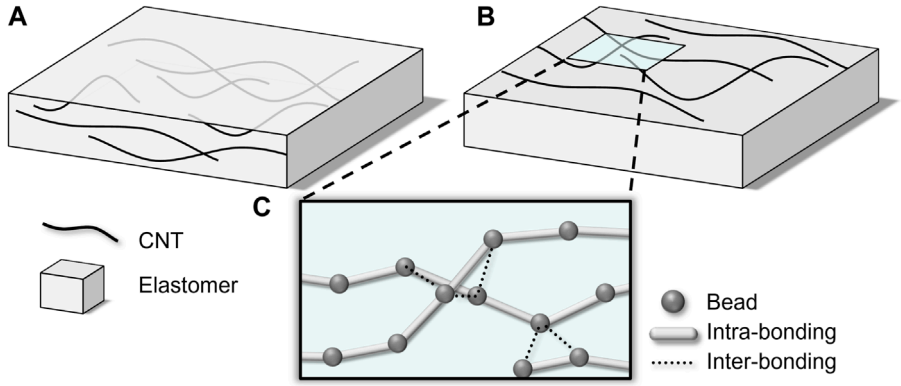

FIGURE 1
Two types of composites in which **(A)** CNT network is embedded in a polymer and **(B)** CNT network is coated on a polymer substrate. **(C)** Configuration of CNT modeled by coarse-grained model.

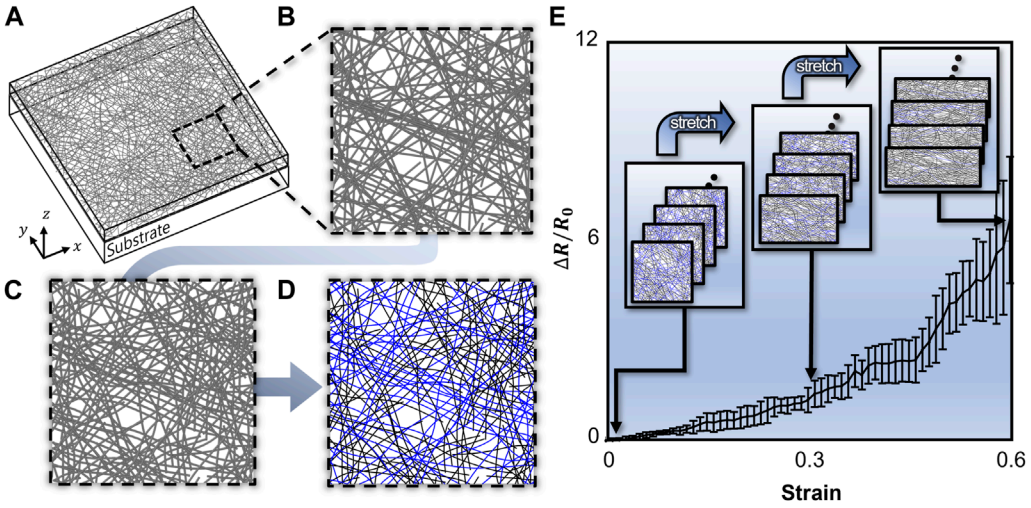

FIGURE 2
(A) Simulation cell for CNT network analysis under periodic boundary conditions along *x* and *y* direction **(B)** Randomly distributed CNT before energy minimization, and **(C)** CNT network after energy minimization. **(D)** CNT network classified percolated (blue) and non-percolated (black) CNT. **(E)** strain *versus* resistance plot drawn for 10 iterations.

where E_i represents the total potential energy at iteration i, and E_{i+1} represents the total potential energy at the next iteration, $i+1$. From the initial distribution of CNT, the CNTs are divided by a length at which the axial direction potential energy is minimum and each segmented position is assigned as a bead. The potential energy of the system is minimized at every stretching step where the simulation box is stretched by strain increment under the constant volume assumption. This process is repeated until the desired strain is reached, and stable distribution of CNT network at each strain is obtained as shown in Figure 2C. In a stable state after energy minimization, it can be seen that the CNTs are bent.

2.3 Percolation network analyses and electric conductivity calculation

From the CNT network configuration obtained from the CGMS simulation, the resistances of the composite are calculated by using the percolation analysis (Lee et al., 2015; Jung et al., 2020). As shown in Figures 3A, B, the lines connecting the two neighboring beads in the same CNT are defined as segments having intrinsic resistance. A distance (d) between two segments that belongs to two different CNT molecules is calculated to classify whether they are in physical contact ($d < d_c$), under tunnel condition ($d_c < d < d_t$),

TABLE 1 **Interatomic potential function for CNT beads.**

Interaction	Potential function
Two beads in the same CNT	$\phi_t(r) = \frac{1}{2}k_t(r_1 - r_0)^2$ where $k_t = 1000$ (kcal/*mol*)/Å^2, $r_0 = 10$ Å
Three beads in the same CNT	$\phi_\theta(\theta) = \frac{1}{2}k_\theta(\theta - \theta_0)^2$ where $k_\theta = 14300$ (kcal/*mol*)/rad^2, $\theta_0 = 180°$
Two beads in different CNTs	$\phi_{Lj}(r_2) = 4\varepsilon\left[\left(\frac{\sigma}{r_2}\right)^{12} - \left(\frac{\sigma}{r_2}\right)^{6}\right]$ where $\varepsilon = 15.1$ *kcal/mol*, $\sigma = 9.35$ Å

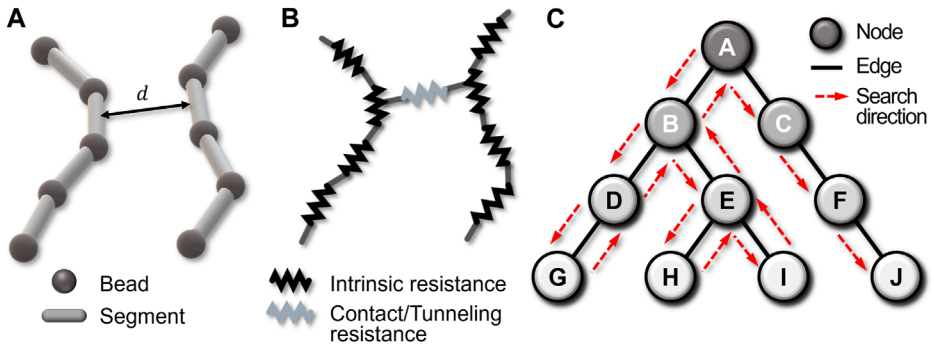

FIGURE 3
(A) CNT network which is represented with a coarse-grained model can be represented as **(B)** a circuit composed of contact/tunneling and intrinsic resistances. **(C)** DFS algorithm scheme; From the given example, the algorithm searches in A-B-D-...-C-F-J node order.

or disconnected ($d > d_t$). Thereafter, contact resistances between the segments are defined depending on the distance as follows,

$$R = \begin{cases} R_c & \text{for } d \le d_c \\ R_t & \text{for } d_c < d \le d_t \\ \infty & \text{for } d > d_t \end{cases} \quad (2)$$

$$where\, R_t = \frac{h}{2e^2}\frac{1}{M}e^{\frac{4\pi(d-d_c)\sqrt{2m\lambda}}{h}} \quad (3)$$

where d_c is contact cutoff distance, d_t is tunneling cutoff distance, R_c is contact resistance, and R_t is tunneling resistance which is used to consider current paths due to quantum tunneling conductive junctions. For the simplification of the simulation, we utilized the Landauer formula depending on the shortest distance as shown in Eq. **3** (Büttiker et al., 1985) where h, e, M, m, and λ are Plank constant, electron charge, number of conduction channel, electron mass, and tunneling energy barrier (Simmons, 1963; Forro and Schoenenberger, 2001; Zhu et al., 2012; Klimm and Kwok, 2022). The distance d_c is determined by the CNT radius. We assumed that a resistance value of 30 times the contact resistance was large enough to be negligible for calculating conductivity of percolated network, so the distance at which tunneling resistance becomes 30 times the contact resistance between CNTs is chosen as the tunneling cutoff distance, d_t. The conductivity of the matrix is ignored because the resistivity of the matrix is much higher compared to that of CNT. The calculation of resistances between all CNT segments is conducted and connectivity between each pair of nodes is examined. Then, a connectivity matrix (***P***) is formed, P_{ij} is allocated 1 or 0 if *i*th segment and *j*th segment are connected or not, respectively.

Because a CNT segment has only a few connections with other CNT segments, most components of the connectivity matrix are zero, thus the matrix is regarded as a sparse matrix. To eliminate unnecessary information, we introduce a dictionary of key format that contains only positions and values of non-zero components. Consequently, the required memory for connectivity information is dramatically reduced. When the volume fraction and CNT length are 0.16 vol% and 600 nm, respectively, 97% less memory was used for the connectivity matrix.

After that, the depth-firsts search (DFS) algorithm is utilized to find clustered CNTs as shown in Figure 3C. A connectivity graph can be constructed from connectivity information. Each node and edge represent a CNT segment and connectivity between CNT segments, respectively. DFS algorithm starts at an arbitrary node and explores as far as possible along each branch as shown in the red arrows of Figure 3C. If the exploration is no longer available, the algorithm explores backward on the same path to find other nodes to traverse. In the algorithm, CNTs that do not form percolating clusters are filtered out, and only CNT clusters contacted with both sides of walls are extracted as shown in Figure 2D.

Finally, the resistance of CNT-elastomer nanocomposite can be obtained by constructing a matrix containing the clustering information of the CNTs and using Kirchhoff's law which dictates that the sum of the incoming and outgoing currents to any node in the circuit is zero. The relationship between resistance and voltage for *i*th node is expressed as follows,

$$\sum I = I_1 + I_2 + \ldots + I_n = 0 \quad (4)$$

$$\sum I = \frac{(V_1 - V_i)}{R_1} + \frac{(V_2 - V_i)}{R_2} + \ldots + \frac{(V_n - V_i)}{R_n} = 0 \quad (5)$$

$$\frac{V_1}{R_1} + \frac{V_2}{R_2} + \cdots + \frac{V_n}{R_n} - V_i\left(\frac{1}{R_1} + \frac{1}{R_2} + \cdots + \frac{1}{R_n}\right) = 0 \quad (6)$$

$$A_{i1}V_1 + A_{i2}V_2 + A_{i3}V_3 + \cdots + A_{in}V_n - A_{ii}V_i = 0 \quad (7)$$

where I_k is an electric current flowing into a node connected with n nodes, V_k is the electric potential level of the kth node. Based on Eq. 6, the following matrix equation can be obtained.

$$\boldsymbol{AV} = \boldsymbol{B} \quad (8)$$

$$\text{where } A_{ij} = \frac{1}{R_j}, A_{ii} = \frac{1}{R_1} + \frac{1}{R_2} + \frac{1}{R_3} + \cdots + \frac{1}{R_n} \quad (9)$$

where $\boldsymbol{A}$ is the conductance matrix, $\boldsymbol{V}$ is the voltage vector, and $\boldsymbol{B}$ is the source vector. $\boldsymbol{A}$ and $\boldsymbol{B}$ are obtained from resistance information and current source, respectively. The kth component of vector $\boldsymbol{B}$ has a value of assigned voltage. Components of vector $\boldsymbol{B}$ other than the nodes touching either constant voltage boundary are zero, and $\boldsymbol{V}$ indicates the voltage at each node, which is solved using a Cholesky decomposition algorithm for sparse matrices.

3 Result

Before applying the proposed model for investigating the effect of design variables, our model is validated against an experimental measurement of the piezoresistive response of spray-coated carbon nanotubes on PDMS substrates (Lipomi et al., 2011). The length and volume fraction of CNT are set up to 2,400 *nm* and 0.18 *vol%*, respectively. As shown in the Figure 4, the average of the estimated value from proposed model is not completely consistent with the experimental results, but the same tendency is shown. And, it is confirmed that the error range of prediction increases because of variability and uncertainty due to randomly dispersed initial CNTs. The experimental result falls within the model's error bounds, demonstrating that the suggested model covers experiments. So, it could be said the numerical analysis matches well with experiments except for a slight discrepancy at the finite strain range. Hence, we can conclude that the proposed model is reasonable to predict the effect of CNT length and volume fraction on the piezoresistivity.

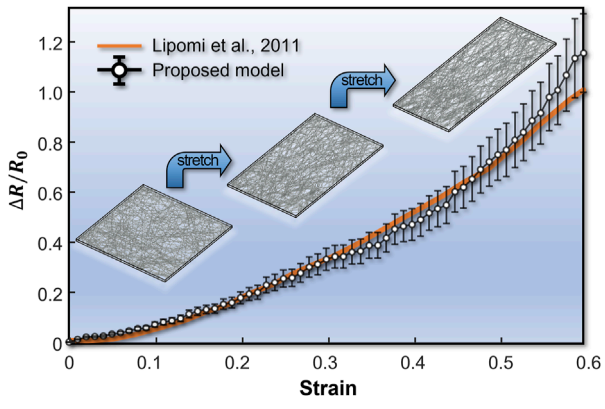

FIGURE 4
Strain *versus* $\Delta R/R_0$ plot for comparison of the experimental results (Lipomi et al., 2011) and prediction of the numerical model. Composites are stretched up to 0.6 strain, in which the length and volume fraction of CNT are 2,400 *nm* and 0.18 *vol%*, respectively.

3.1 Effect of volume fraction of CNT

To unveil the effect of the CNT volume fraction, the simulation is conducted by changing only the volume fraction while the other design conditions are kept fixed. i.e., length and diameter of CNT are 300 *nm* and 1 *nm*, respectively. As depicted in Figure 5A, a similar linear piezoresistive response is observed in the small strain regime ($\varepsilon < 1.0$), regardless of volume fraction. In contrast, in the large strain regime ($\varepsilon > 1.0$), the nonlinearity in the piezoresistive response increases with the reduction of volume fraction. The initiation of nonlinear behavior became faster with a smaller volume fraction of CNT for fixed length and diameter of CNT. To unveil the mechanism behind the volume fraction dependence, we visualize the change of CNT network in Figures 5B, C. For the composite with high volume fractions, CNTs are distributed relatively uniformly regardless of applied strain. On the other hand, with the reduction of volume fraction, the percolated CNTs are more rapidly diminished as strain increases, which leads to the occurrence of bottlenecks in the percolation network. This is because, when the volume fraction of carbon nanotubes (CNTs) in a network is lower, the interparticle interactions between CNTs are weakened. This weakening of interactions can make agglomeration more likely to occur. Such bottlenecks in the percolation network cause nonlinear piezoresistive behavior.

3.2 Effect of length of CNT

We also analyzed the piezoresistive response of the CNT composites by varying CNT length and investigated its effect on the piezoresistive response. Here, the volume fraction and diameter of CNT are 0.78 *vol%* and 1 nm, respectively. Similar to the previous section, in the small strain regime, a linear piezoresistive response is observed regardless of CNT length as shown in Figure 6A. On the other hand, in the high strain regime, composites consisting of shorter CNT fibers show a nonlinear increase of resistance with the strain, whereas composites with longer CNT fibers sustain linear response longer. Figures 6B, C shows that such a nonlinear response originates from the bottleneck in the percolation network topology. This is because the CNT length gets shorter, the percolation network is more sparsely connected and becomes less persistent over the stretch making agglomeration more likely to occur. In short, the initiation of nonlinear behavior became faster with a smaller length of CNT for fixed volume fraction and diameter of CNT.

3.3 Performance map

Using the proposed numerical model, we modeled the piezoresistive response for 51 different combinations of volume fraction and length to generate a performance map in Figure 7. Figure 7A visualizes the maximum strain at which the composite has a linear piezoresistive response, which can be interpreted as the stretchability of the sensor. The stretchability is interpreted by the linearly stretchable range and defined as the maximum strain with R^2 value greater than 0.98 in 1st order polynomial curve

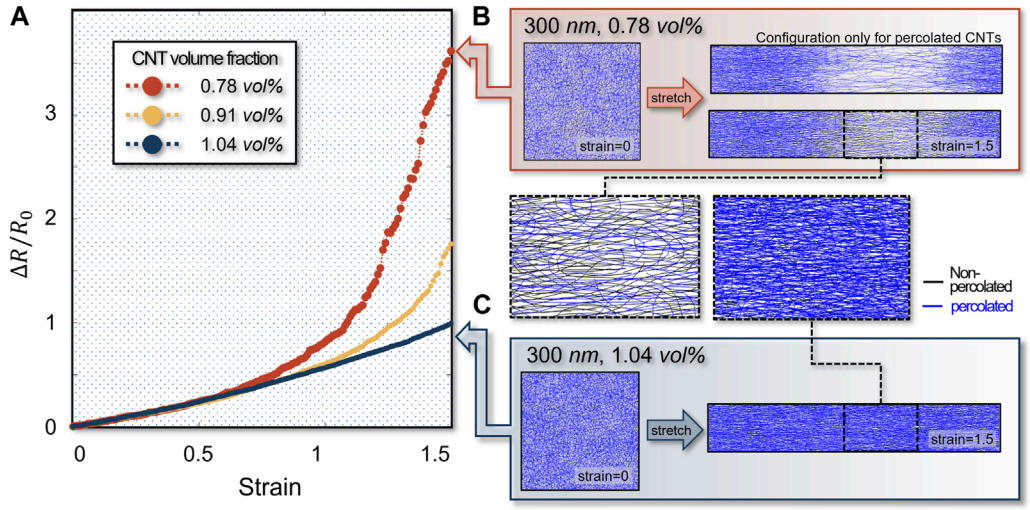

FIGURE 5
(A) Strain *versus* $\Delta R/R_0$ plot according to the volume fraction of CNT when the length and the diameter of CNT are 300 *nm* and 1 *nm*, respectively. The microstructural of CNT network when the volume fraction of CNT is **(B)** 0.78 *vol%* and **(C)** 1.04 *vol%*, respectively.

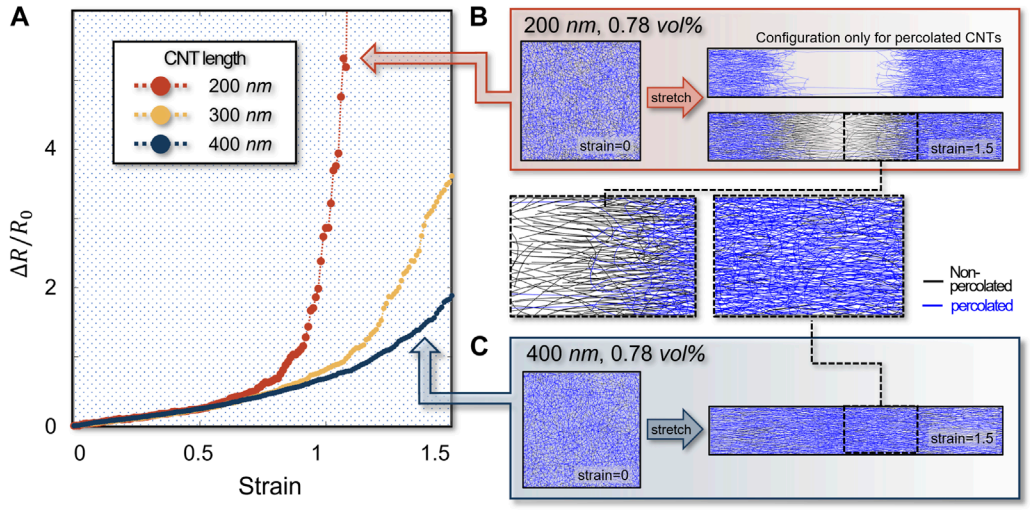

FIGURE 6
(A) Strain *versus* $\Delta R/R_0$ plot according to the length of CNT when the volume fraction and the diameter of CNT are 0.78 *vol%* and 1 *nm*. The microstructural of the CNT network is presented when the lengths of CNT are **(B)** 200 *nm* and **(C)** 400 *nm*, respectively.

fitting. Figure 7B presents the gauge factor ($\Delta R/\varepsilon$) of the strain *versus* resistance curve within the linear response regime. In other words, Figures 7A, B represent the stretchability and sensitivity of the piezoresistive sensors made of CNT-elastomer nanocomposites. The range where the piezoresistive response is not calculated via the numerical model was recovered by linear interpolation.

In the very low volume fraction or short length regime (lower left corner of the performance map), there is no piezoresistivity because no percolation network is formed. In the very large volume fraction and long length regime, the percolation network is very densely connected. Despite very high stretchability, the predicted sensitivity is low because the uniformly connected percolation network persists until a large mechanical strain is applied. In the volume fraction and length ranges just above the percolation threshold (a convex region connecting the upper left corner to the lower right corner), the gauge factor is very large because the percolation network topology changes significantly over the strain, but its stretchability is very limited. Overall, the performance map shows the trade-off relationship between the stretchability and the sensitivity (i.e., gauge factor). The performance map can serve as

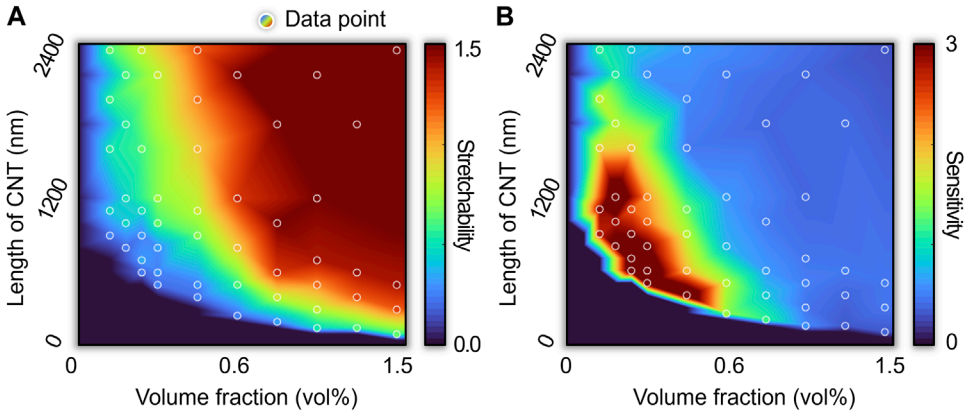

FIGURE 7
(A) Stretchability and **(B)** sensitivity map when volume fraction and length of CNT are design parameters. The lower left region forms a non-percolation network. The stretchability is defined as linearly stretchable range. The sensitivity is represented by a gauge factor within linear response range.

a guideline for designing the piezoresistive sensors to achieve the desired stretchability and sensitivity by considering the performance limit.

4 Conclusion

In this research, based on an efficient numerical model for predicting the piezoresistivity response of coated CNT network-based nanocomposites, we constructed a performance map featuring stretchability and sensitivity. Based on an efficient sparse matrix-based algorithm, we reduce the computing time for percolation analyses, which enabled us to effectively obtain the piezoresistive response in a large strain range for a variety of combinations of volume fraction and length of CNT. First, we show that the piezoresistive response predicted from our simulation model matches well with existing experimental measurements. Second, we identify the microscopic origin behind the transition between linear and nonlinear piezoresistive response upon volume fraction or length change. Moreover, we construct the strain sensing performance map showing the stretchability and sensitivity over a wide range of volume fractions and lengths, which has not been explored in detail so far. We expect that the performance map can serve as a guideline to design CNT-elastomer nanocomposite piezoresistive sensors.

Data availability statement

The raw data supporting the conclusion of this article will be made available by the authors, without undue reservation.

Author contributions

JY and SR contributed to conception and design of the study. JY implemented simulation code, collected data, and analyzed the result under the guidance of SR. JJ provided feedback and helped shape the research. JY wrote the first draft of the manuscript with support from JJ. All authors contributed to the article and approved the submitted version.

Funding

This work is financially supported by the National Research Foundation of Korea (NRF) (2022R1A2B5B02002365).

Conflict of interest

The authors declare that the research was conducted in the absence of any commercial or financial relationships that could be construed as a potential conflict of interest.

Publisher's note

References

Amjadi, M., Pichitpajongkit, A., Lee, S., Ryu, S., and Park, I. (2014). Highly stretchable and sensitive strain sensor based on silver nanowire–elastomer nanocomposite. *ACS nano* 8, 5154–5163. doi:10.1021/nn501204t

Buehler, M. J. (2006). Mesoscale modeling of mechanics of carbon nanotubes: Self-assembly, self-folding, and fracture. *J. Mater. Res.* 21, 2855–2869. doi:10.1557/jmr.2006.0347

Büttiker, M., Imry, Y., Landauer, R., and Pinhas, S. (1985). Generalized many-channel conductance formula with application to small rings. *Phys. Rev. B* 31, 6207–6215. doi:10.1103/physrevb.31.6207

Chen, Y., Zimmerman, J., Krivtsov, A., and Mcdowell, D. L. (2011). Assessment of atomistic coarse-graining methods. *Int. J. Eng. Sci.* 49, 1337–1349. doi:10.1016/j.ijengsci.2011.03.018

DE Vivo, B., Lamberti, P., Spinelli, G., Tucci, V., Vertuccio, L., and Vittoria, V. (2014). Simulation and experimental characterization of polymer/carbon nanotubes composites for strain sensor applications. *J. Appl. Phys.* 116, 054307. doi:10.1063/1.4892098

Farooq, M., and Sazonov, E. (2015). *Wearable Electronics sensors*. Springer. Strain sensors in wearable devices.

Fish, J., Wagner, G. J., and Keten, S. (2021). Mesoscopic and multiscale modelling in materials. *Nat. Mater.* 20, 774–786. doi:10.1038/s41563-020-00913-0

Forro, L., and Schoenenberger, C. (2001). *Physical properties of multi-wall nanotubes. Carbon nanotubes: Synthesis, structure, properties, and applications*. Springer.

Gorban, A. N., and Karlin, I. V. (2002). Macroscopic dynamics through coarse-graining: A solvable example. *Phys. Rev. E* 65, 026116. doi:10.1103/physreve.65.026116

Grujicic, M., Cao, G., and Roy, W. (2004). A computational analysis of the percolation threshold and the electrical conductivity of carbon nanotubes filled polymeric materials. *J. Mater. Sci.* 39, 4441–4449. doi:10.1023/b:jmsc.0000034136.11779.96

Haghgoo, M., Hassanzadeh-Aghdam, M., and Ansari, R. (2020). A comprehensive evaluation of piezoresistive response and percolation behavior of multiscale polymer-based nanocomposites. *Compos. Part A Appl. Sci. Manuf.* 130, 105735. doi:10.1016/j.compositesa.2019.105735

Helmer, R., Farrow, D., Ball, K., Phillips, E., Farouil, A., and Blanchonette, I. (2011). A pilot evaluation of an electronic textile for lower limb monitoring and interactive biofeedback. *Procedia Eng.* 13, 513–518. doi:10.1016/j.proeng.2011.05.123

Hu, B., Hu, N., Li, Y., Akagi, K., Yuan, W., Watanabe, T., et al. (2012). Multi-scale numerical simulations on piezoresistivity of CNT/polymer nanocomposites. *Nanoscale Res. Lett.* 7, 402–411. doi:10.1186/1556-276x-7-402

Hu, N., Fukunaga, H., Atobe, S., Liu, Y., and Li, J. (2011). Piezoresistive strain sensors made from carbon nanotubes based polymer nanocomposites. *Sensors* 11, 10691–10723. doi:10.3390/s111110691

Hu, N., Masuda, Z., Yan, C., Yamamoto, G., Fukunaga, H., and Hashida, T. (2008). The electrical properties of polymer nanocomposites with carbon nanotube fillers. *Nanotechnology* 19, 215701. doi:10.1088/0957-4484/19/21/215701

Huo, Q., Jin, J., Wang, X., Lu, S., Zhang, Y., Ma, J., et al. (2019). Preparation of graphene-based sensor and its application in human behavior monitoring. *Mater. Res. Express* 6, 075613. doi:10.1088/2053-1591/ab17ac

Jin, L., Chortos, A., Lian, F., Pop, E., Linder, C., Bao, Z., et al. (2018). Microstructural origin of resistance-strain hysteresis in carbon nanotube thin film conductors. *Proc. Natl. Acad. Sci. U. S. A.* 115, 1986–1991. doi:10.1073/pnas.1717217115

Jung, J., Lee, S., Pugno, N. M., and Ryu, S. (2020). Orientation distribution dependence of piezoresistivity of metal nanowire-polymer composite. *Multiscale Sci. Eng.* 2, 54–62. doi:10.1007/s42493-020-00035-4

Jung, S., Choi, H. W., Mocanu, F. C., Shin, D.-W., Chowdhury, M. F., Han, S. D., et al. (2019). Modeling electrical percolation to optimize the electromechanical properties of CNT/polymer composites in highly stretchable fiber strain sensors. *Sci. Rep.* 9, 20376–20410. doi:10.1038/s41598-019-56940-8

Kang, I., Schulz, M. J., Kim, J. H., Shanov, V., and Shi, D. (2006). A carbon nanotube strain sensor for structural health monitoring. *Smart Mater. Struct.* 15, 737–748. doi:10.1088/0964-1726/15/3/009

Klimm, W., and Kwok, K. (2022). Tunneling resistance model for piezoresistive carbon nanotube polymer composites. *Nanotechnology* 34, 045502. doi:10.1088/1361-6528/ac9c0d

Kwon, D., Lee, T. I., Shim, J., Ryu, S., Kim, M. S., Kim, S., et al. (2016). Highly sensitive, flexible, and wearable pressure sensor based on a giant Piezocapacitive effect of three-Dimensional Microporous elastomeric Dielectric Layer. *ACS Appl. Mater Interfaces* 8, 16922–16931. doi:10.1021/acsami.6b04225

Lee, S., Amjadi, M., Pugno, N., Park, I., and Ryu, S. (2015). Computational analysis of metallic nanowire-elastomer nanocomposite based strain sensors. *AIP Adv.* 5, 117233. doi:10.1063/1.4936635

Levitt, M. (1976). A simplified representation of protein conformations for rapid simulation of protein folding. *J. Mol. Biol.* 104, 59–107. doi:10.1016/0022-2836(76)90004-8

Li, J., and Kim, J.-K. (2007). Percolation threshold of conducting polymer composites containing 3D randomly distributed graphite nanoplatelets. *Compos. Sci. Technol.* 67, 2114–2120. doi:10.1016/j.compscitech.2006.11.010

Lipomi, D. J., Vosgueritchian, M., Tee, B. C., Hellstrom, S. L., Lee, J. A., Fox, C. H., et al. (2011). Skin-like pressure and strain sensors based on transparent elastic films of carbon nanotubes. *Nat. Nanotechnol.* 6, 788–792. doi:10.1038/nnano.2011.184

Liu, C.-X., and Choi, J.-W. (2009). "An embedded PDMS nanocomposite strain sensor toward biomedical applications," in Annual International Conference of the IEEE Engineering in Medicine and Biology Society (IEEE), 6391–6394.

Lorussi, F., Scilingo, E. P., Tesconi, M., Tognetti, A., and DE Rossi, D. (2005). Strain sensing fabric for hand posture and gesture monitoring. *IEEE Trans. Inf. Technol. Biomed.* 9, 372–381. doi:10.1109/titb.2005.854510

Lu, N., Lu, C., Yang, S., and Rogers, J. (2012). Highly sensitive skin-mountable strain gauges based entirely on elastomers. *Adv. Funct. Mater.* 22, 4044–4050. doi:10.1002/adfm.201200498

Lu, S., DU, K., Wang, X., Tian, C., Chen, D., Ma, K., et al. (2019). Real-time monitoring of low-velocity impact damage for composite structures with the omnidirection carbon nanotubes' buckypaper sensors. *Struct. health Monit.* 18, 454–465. doi:10.1177/1475921718757937

Mora, A., Verma, P., and Kumar, S. (2020). Electrical conductivity of CNT/polymer composites: 3D printing, measurements and modeling. *Compos. Part B Eng.* 183, 107600. doi:10.1016/j.compositesb.2019.107600

Njuguna, M., Yan, C., Hu, N., Bell, J., and Yarlagadda, P. (2012). Sandwiched carbon nanotube film as strain sensor. *Compos. Part B Eng.* 43, 2711–2717. doi:10.1016/j.compositesb.2012.04.022

Obitayo, W., and Liu, T. (2012). A review: Carbon nanotube-based piezoresistive strain sensors. *J. Sensors*, 2012, 1–15. doi:10.1155/2012/652438

Plimpton, S. (1995). Fast parallel algorithms for short-range molecular dynamics. *J. Comput. Phys.* 117, 1–19. doi:10.1006/jcph.1995.1039

Seidel, G. D., and Lagoudas, D. C. (2009). A micromechanics model for the electrical conductivity of nanotube-polymer nanocomposites. *J. Compos. Mater.* 43, 917–941. doi:10.1177/0021998308105124

Simmons, J. G. (1963). Generalized formula for the electric tunnel effect between similar electrodes separated by a thin insulating film. *J. Appl. Phys.* 34, 1793–1803. doi:10.1063/1.1702682

Song, Z., Li, W., Bao, Y., Han, F., Gao, L., Xu, J., et al. (2018). Breathable and skin-mountable strain sensor with tunable stretchability, sensitivity, and Linearity via Surface strain Delocalization for versatile skin Activities' Recognition. *ACS Appl. Mater Interfaces* 10, 42826–42836. doi:10.1021/acsami.8b14365

Sun, X., Qin, Z., Ye, L., Zhang, H., Yu, Q., Wu, X., et al. (2020). Carbon nanotubes reinforced hydrogel as flexible strain sensor with high stretchability and mechanically toughness. *Chem. Eng. J.* 382, 122832. doi:10.1016/j.cej.2019.122832

Taya, M., Kim, W., and Ono, K. (1998). Piezoresistivity of a short fiber/elastomer matrix composite. *Mech. Mater.* 28, 53–59. doi:10.1016/s0167-6636(97)00064-1

Wang, X., Lu, S., Ma, K., Xiong, X., Zhang, H., and Xu, M. (2015). Tensile strain sensing of buckypaper and buckypaper composites. *Mater. Des.* 88, 414–419. doi:10.1016/j.matdes.2015.09.035

Xiao, X., Yuan, L., Zhong, J., Ding, T., Liu, Y., Cai, Z., et al. (2011). High-strain sensors based on ZnO nanowire/polystyrene hybridized flexible films. *Adv. Mater.* 23, 5440–5444. doi:10.1002/adma.201103406

Yamada, T., Hayamizu, Y., Yamamoto, Y., Yomogida, Y., Izadi-Najafabadi, A., Futaba, D. N., et al. (2011). A stretchable carbon nanotube strain sensor for human-motion detection. *Nat. Nanotechnol.* 6, 296–301. doi:10.1038/nnano.2011.36

Zhang, J., Liu, J., Zhuang, R., Mäder, E., Heinrich, G., and Gao, S. (2011). Single MWNT-glass fiber as strain sensor and switch. *Adv. Mater.* 23, 3392–3397. doi:10.1002/adma.201101104

Zhu, Y., Qin, Q., Xu, F., Fan, F., Ding, Y., Zhang, T., et al. (2012). Size effects on elasticity, yielding, and fracture of silver nanowires: *In situ* experiments. *Phys. Rev. B* 85, 045443. doi:10.1103/physrevb.85.045443